Development Status of a 3-D Electron Fluid Model for Hall Thruster Plume Simulations

Maria Choi[1] and John T. Yim[2]
NASA Glenn Resarch Center, Cleveland, OH, 44135

A 3-D electron fluid model has been developed as a stepping stone to fully describe the electron current flow across magnetic fields inside a vacuum chamber and to provide electron flux to solar arrays for spacecraft surface charging model. A detailed description of the numerical treatment of the electric potential solver, including finite-volume formulation, implementation, and the treatment of boundary conditions, are presented in this paper. Verification tests of the model are presented.

Nomenclature

$\boldsymbol{B}$	=	magnetic fields
e	=	elementary charge
$\boldsymbol{E}$	=	electric fields
N_x, N_y, N_z	=	number of cells in the *x*-, *y*-, *z*-directions
n_e	=	electron number density
$\hat{n}$	=	normal vector
$\boldsymbol{j}_e$	=	electron current density
$\boldsymbol{j}_i$	=	ion current density
P_e	=	electron pressure
S	=	surface
V	=	cell volume
σ_e	=	electron conductivity
μ_e	=	electron mobility
$\bar{\bar{\mu}}$	=	electron mobility tensor
ϕ	=	plasma potential
ϕ_w	=	wall potential

I. Introduction

IN order to better understand the testing environment of ground based vacuum chambers, it is critical not only to understand the motion of heavy particles in the plume, but also the movement of bulk electron flows. While the background pressure effects have been extensively studied in the past, [1-6] there is still limited understanding of how electrons in the plume of electric propulsion (EP) thrusters travel through and interact with the metallic conductive walls of vacuum chambers. Recent studies have suggested that the presence of conducting walls provides alternate pathways for electrons to travel from the cathode and serve as a recombination site.[7-8] This electrical facility effect can become more significant for higher-power thrusters operating in vacuum facilities. However, this effect is absent in orbit and thus needs to be understood as simulations are most often validated through comparisons with ground facility measurement data.

A conventional way to simulate electrons in the plume of EP thrusters is to assume the Boltzmann relation. This method is simple and useful for isothermal, collisionless, and unmagnetized regions, but has major limitations for Hall thruster plume simulations. First, the electron temperature gradient in the plume is not negligible as they can vary by more than an order of magnitude from the near-field to the far-field. Second, the magnetic field strength is still strong in the near-field plume, as the field leaks into the plume. In order to improve the fidelity of electron model, early work

[1] R&D Engineer, Electric Propulsion Systems Branch, maria.choi@nasa.gov.
[2] R&D Engineer, Electric Propulsion Systems Branch, john.t.yim@nasa.gov.

by Boyd and Yim[9] demonstrated the viability of using a current conservation / Ohm's Law approach to solve for electron current flows for a Hall thruster plume, assuming negligible magnetic fields. This work was further demonstrated on a cluster of Hall thruster plumes by Cai and Boyd.[10] In both cases, the authors demonstrated difference in plume structures between their approach and the traditional Boltzmann relation approximation used in plume codes—which enforces exactly zero electron current everywhere in the plume such as the Coliseum tool described by Brieda and VanGilder.[11] The work by Ref. 9-10 was further improved by Choi and Boyd[12] by including a full electron mobility tensor to account for anisotropies in electron transport in vacuum chamber due to magnetic field effects. This study used in a 2-D axisymmetric unstructured mesh and showed that the magnetic field effects are non-negligible in the near-field plumes of the anode and cathode.

The present work utilizes the formulation by Choi and Boyd[12] using a cell-centered finite volume method in 3-D Cartesian mesh. The ultimate goal of this work is to better understand electrical effects of a conducting vacuum chamber and provide electron current flux to a surface charging model[13] that has been developed by the Air Force Research Laboratory (AFRL) at Edwards. In this paper, the full electron mobility tensor, $\bar{\bar{\mu}}$, as in Ref. 4, and a full representation of the electron current density, j_e, in 3-D Cartesian grids is developed and presented to better understand the electron transport and current flow in a vacuum chamber. Using the Generalized Ohm's law and the steady-state current conservation equation, the electric potential is derived.

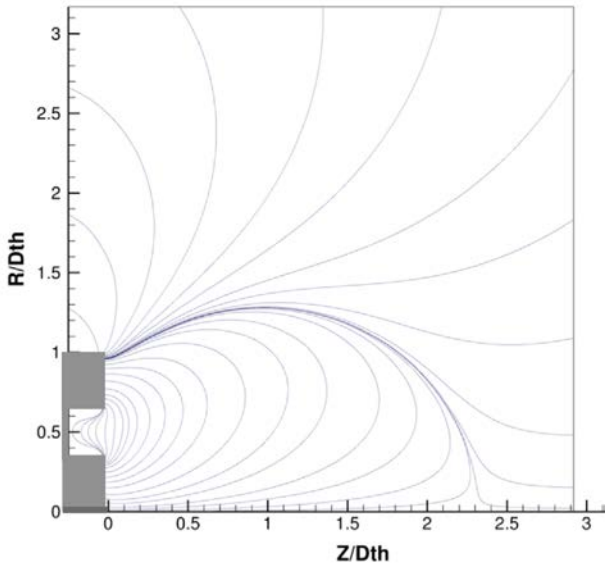

Figure 1. Complex magnetic field lines in a Hall thruster [12].

The new electron model has a capability to model electron transport across a complex magnetic field topology in the plume, which includes a magnetic field separatrix and a purely axial component along the cathode centerline axis and a purely radial component near the discharge channel exit, as shown in Fig. 1. A detailed description of the numerical treatment of the electric potential solver, including finite-volume formulation, implementation, and treatment of boundary conditions, are provided in the paper. Boundary conditions include a representative ion source representing a Hall thruster, and potential boundary conditions (Dirichlet for all metallic surfaces including chamber wall, and Neumann for dielectric thruster body). This approach will ultimately be integrated into a hybrid PIC plume code and will be used to map out the electrostatic potential and the electron current flows through the chamber volume of a Hall thruster firing in a vacuum chamber.

Before simulating a full thruster, the model is verified using the method of manufactured solutions and a mock Hall thruster testcase. The simulation results will be compared against various measured data. The accuracy of the new model and effect of magnetic field in the near-field plume will be discussed.

II. Physical and Numerical Models

For a fluid description for the electron plasma, the generalized Ohm's law and the steady state current conservation equation are derived as follows:

$$\boldsymbol{j}_e = \mu_e(\boldsymbol{j}_e \times \boldsymbol{B}) + \sigma_e\left(\boldsymbol{E} + \frac{1}{en_e}\nabla P_e\right) \tag{1}$$

$$\nabla \cdot (\boldsymbol{j}_e + \boldsymbol{j}_i) = 0 \tag{2}$$

where $\boldsymbol{j}_e$ and $\boldsymbol{j}_i$ are the electron and ion current densities, respectively, $\boldsymbol{B}$ is the magnetic field, $\boldsymbol{E}$ is the electric field, σ_e is the electron conductivity, n_e is the electron number density, P_e is the electron pressure assuming ideal gas, and μ_e is the electron mobility defined as:

$$\mu_e = \frac{q}{m_e \nu_{ce}}$$

with q being the elementary charge, m_e the electron mass, and ν_{ce} the total collision frequency of the electron fluid. Introducing plasma potential ϕ in relation to the electric field, $-\nabla\phi = \boldsymbol{E}$, Eq.(1) can be re-written as follows:

$$\bar{\bar{\mu}}\boldsymbol{j}_e = \sigma_e\left(-\nabla\phi + \frac{1}{en_e}\nabla P_e\right) \tag{3}$$

where $\bar{\bar{\mu}}$ is the mobility tensor,

$$\bar{\bar{\mu}} = \begin{bmatrix} 1 & -\mu_e B_x & \mu_e B_z \\ \mu_e B_x & 1 & -\mu_e B_y \\ -\mu_e B_z & \mu_e B_y & 1 \end{bmatrix}$$

Combining Eq. (3) with Eq. (2), we obtain the following equation to solve for the plasma potential:

$$\nabla\cdot(\bar{\bar{\mu}}^{-1}\sigma_e\nabla\phi) = \nabla\cdot\left(\bar{\bar{\mu}}^{-1}\frac{\sigma_e}{en_e}\nabla P_e\right) + \nabla\cdot\boldsymbol{j}_i \tag{4}$$

where $\bar{\bar{\mu}}^{-1}$ is the inverse of the electron mobility tensor,

$$\bar{\bar{\mu}}^{-1} = \frac{1}{1+\mu_e^2|B|^2}\begin{bmatrix} 1+\mu_e^2B_x^2 & \mu_e^2B_xB_y+\mu_eB_z & \mu_e^2B_xB_z+\mu_eB_y \\ \mu_e^2B_xB_y-\mu_eB_z & 1+\mu_e^2B_y^2 & \mu_e^2B_yB_z+\mu_eB_x \\ \mu_e^2B_xB_z+\mu_eB_y & \mu_e^2B_yB_z-\mu_eB_x & 1+\mu_e^2B_y^2 \end{bmatrix}$$

A cell-centered finite volume method is used to discretize the governing equation in Eq. (4) inside a control volume, V, as follows:

$$\int_V [\nabla\cdot(\bar{\bar{\mu}}^{-1}\sigma_e\nabla\phi)]dV = \int_V \left[\nabla\cdot\left(\bar{\bar{\mu}}^{-1}\frac{\sigma_e}{en_e}\nabla P_e\right)\right]dV + \int_V (\nabla\cdot\boldsymbol{j}_i)dV \tag{5}$$

The volume integrals is transformed as surface integrals using the Green's theorem. Then, the surface integral is approximated as the sum of all fluxes along all faces. In 3-D, this operation for the left hand term of Eq. (5) will be:

$$\sum_{q}^{All\ Faces} (\sigma\bar{\bar{\mu}}^{-1}\nabla\phi)_q\cdot(\hat{n}dS)_q$$
$$= (\sigma\bar{\bar{\mu}}^{-1}\nabla\phi)_e\cdot(\hat{n}dS)_e + (\sigma\bar{\bar{\mu}}^{-1}\nabla\phi)_n\cdot(\hat{n}dS)_n + (\sigma\bar{\bar{\mu}}^{-1}\nabla\phi)_w\cdot(\hat{n}dS)_w + (\sigma\bar{\bar{\mu}}^{-1}\nabla\phi)_s\cdot(\hat{n}dS)_s$$
$$+ (\sigma\bar{\bar{\mu}}^{-1}\nabla\phi)_b\cdot(\hat{n}dS)_b + (\sigma\bar{\bar{\mu}}^{-1}\nabla\phi)_f\cdot(\hat{n}dS)_f$$

where subscripts e, w, n, s, f, and b represents east, west, north, south, front, and back faces, repectively. The final discretized form of this equation turns out to be identical to a cell-centered finite differencing discretization and has 27 stencils in 3-D (Figure 2a). After discretization, the equation becomes a linear system of equations:

$$a\phi_{ijk} + b\phi_{i+1,jk} + c\phi_{i-1,jk} + d\phi_{j+1,ik} + e\phi_{j-1,ik} + \cdots + h\phi_{i+1j+1} + i\phi_{i+1j-1} + j\phi_{i-1j+1} + \cdots = F_{ijk} \tag{5}$$

where F_{ijk} is the right-hand side term and the coefficients $a, b, c, \ldots$ are flux terms (i.e., $\sigma\bar{\bar{\mu}}^{-1}$) at faces such as e, n, w, s, f and b indicated in red boxes in Figure 2b.

The electron pressure is assumed to be isotropic and follows the ideal gas law. The ion current density information in each control volume is acquired through the particle-in-cell (PIC) method assuming quasi-neutrality. The plasma potential is determined by inverting the matrix. After the plasma potential is calculated, we can solve for the electron current density in Eq. (3):

$$\boldsymbol{j}_e = \bar{\bar{\mu}}^{-1}\sigma_e\left(-\nabla\phi + \frac{1}{en_e}\nabla P_e\right)$$

where the central differencing is used to calculate the derivatives.

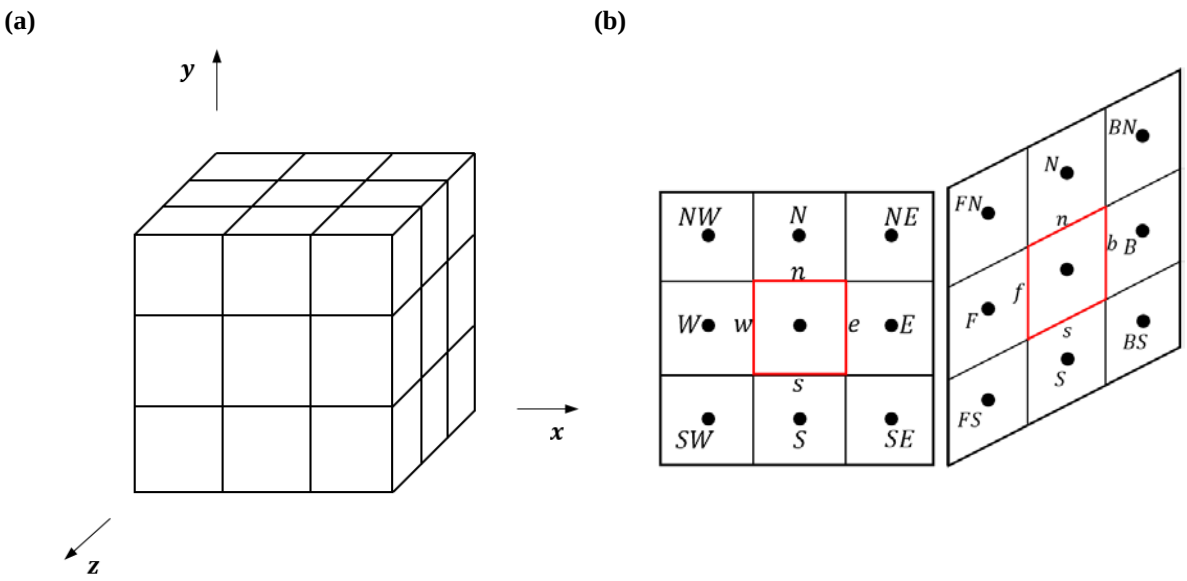

Figure 2. Illustration of (a) 27-point stencils in 3-D rectangular grid, and (b) cell-centers and faces.

III. Boundary Conditions

In Hall thruster plume simulation, typically two types of conditions are used: 1) direct value (e.g., bias-voltage and ground surfaces) and 2) gradient or flux to the surface (e.g., zero-gradient potential), which are Dirichlet and Neumann boundary conditions, respectively. Treatments of these boundary conditions for this model are discussed in this section.

A. Dirichlet Boundary Condition

There are multiple ways to implement Dirichlet boundary condition for the plasma potential. The simplest way is to have the surface on cell-center using a ghost cell (e.g., ϕ_0), as shown in Figure 3(a). Then, the known potential value can be incorporated as a boundary condition by moving the boundary term to the right hand side (RHS) of the equation for interior cells. This method requires modifying all interior cells that have a boundary cell adjacent to them and will result in a matrix with size $(N_x \times N_y \times N_z)$ by $(N_x \times N_y \times N_z)$, where N_x, N_y, and N_z are the number of cells in x-, y-, and z-directions. Instead of this incorporation, the boundary terms can be added in the matrix as additional rows, which preserves the matrix shape of interior cells but increases the matrix to $[(N_x+2)\times(N_y+2)\times(N_x+2)]$ by $[(N_x+2)\times(N_y+2)\times(N_x+2)]$.

When the Dirichlet condition is imposed on a cell-face, instead of a cell-center, as shown in Figure 3(b), either the finite-volume approach or finite-difference approach can be taken. For the finite-volume approach, forward differencing can be at the boundary surface (e.g., $x=\frac{1}{2}$ in Figure 3b) used as follows:

$$\left.\frac{\partial\phi}{\partial x}\right|_{\frac{1}{2}} = \frac{\phi_1 - \phi_{\frac{1}{2}}}{\left(\frac{\Delta x}{2}\right)}$$

For the finite difference approach, the ghost cell ϕ_0 is used and its value is replaced by a known potential value at the wall (i.e., $\phi_{\frac{1}{2}}$), which is approximated using Taylor's expansion. In this study, both 1st order and 2nd order extrapolations are tested, defined as the following:

$$\phi_0 = 2\phi_{\frac{1}{2}} - \phi_1$$

$$\phi_0 = \frac{8}{3}\phi_{\frac{1}{2}} - 2\phi_1 + \frac{1}{3}\phi_2$$

respectively. When approximating the flux at the boundary cell face $(\sigma\bar{\bar{\mu}}^{-1})_{\frac{1}{2}}$, 2nd order extrapolation is used:

$$(\sigma\bar{\bar{\mu}}^{-1})_{\frac{1}{2}} = \frac{3(\sigma\bar{\bar{\mu}}^{-1})_1 - (\sigma\bar{\bar{\mu}}^{-1})_2}{2}$$

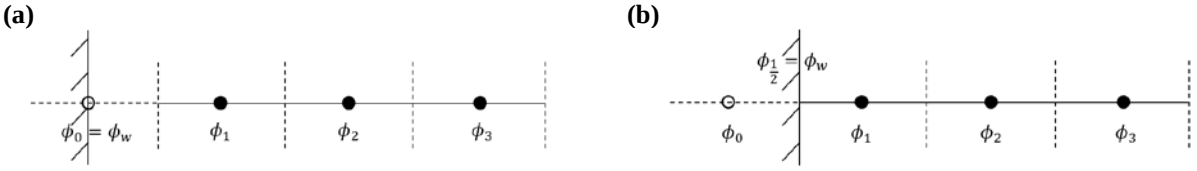

Figure 3. Two types of Dirichlet conditions at a solid surface lying on the (a) cell-center and (b) cell face.

B. Neumann Boundary Condition

For the Neumann boundary condition, our choice for the numerical scheme is limited to 1st order approximation as shown in Figure 4. The ghost cell ϕ_0 is replaced by the known gradient at the cell-face as $\phi_0 = \phi_1 + g_w \Delta x$, which is then used to modify the matrix. For a zero-gradient condition, a mirror condition can be used by setting $\phi_0 = \phi_1$.

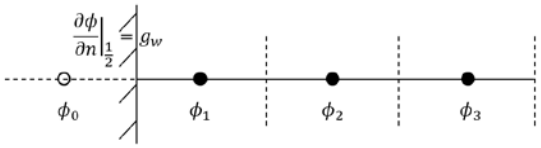

Figure 4. Neumann boundary condition.

IV. Verification Tests

Before implementing this model into a Hall thruster plume code, the model and algorithm have to be tested and verified. In this section, the method of manufactured solutions and a Hall thruster-like testcase are used to verify the model and algorithm.

C. Method of Manufactured Solutions

In order to verify the numerical model, the method of manufactured solution is used. In this study, the new model is tested using various types of functions as manufactured (true) solutions, including polynomial, sinusoidal, and exponential solutions, or some combination of these. The manufactured solution is substituted into the governing equation we are solving numerically, and the source term in the right-hand side is acquired that satisfy this solution. As an example, one of the manufactured solutions tried is shown below:

$$\phi_{exact} = \frac{K}{6}(x^2 + y^2 + z^2)$$

And, the right-hand side is:

$$F = \frac{K}{3}\sigma_e(\mu_{11} + \mu_{22} + \mu_{33})$$

where $K = 3$. The numerical and exact solutions are compared in Figure 5. The numerical solution calculated using the new model qualitatively reproduces the exact solution very well.

For more quantitative study, a grid convergence study can be performed using the L_2-norm error:

$$\|e\|_{L2} = \sqrt{\sum_{k=1}^{N_k} \int_{\Omega_k} (\phi_h - \phi_{exact})^2 d\Omega_k}$$

where ϕ_h is the numerical value of the plasma potential and ϕ_{exact} is the true solution. The convergence study is performed as shown in Figure 6, which confirms the 2nd order accuracy, incidated by the slope of the linear plot (≈ -2).

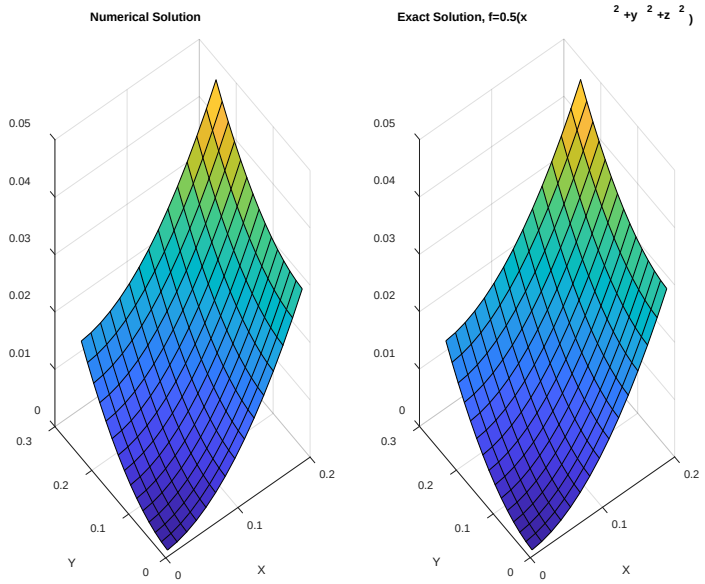

Figure 5. Qualitative comparison of the numerical solution and the exact (manufactured) solution.

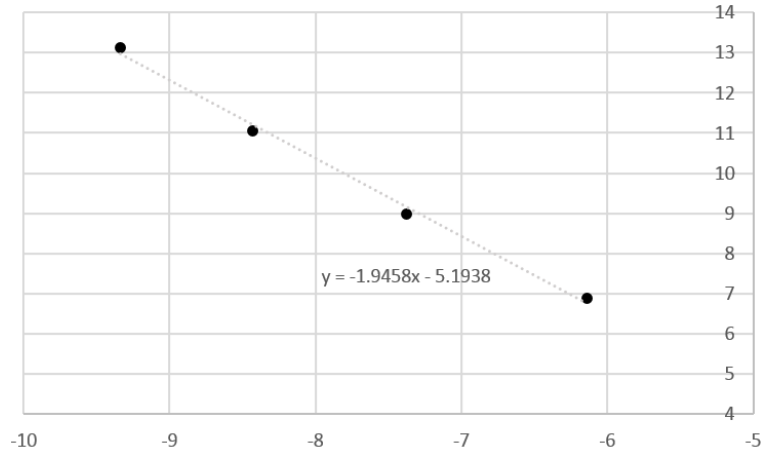

Figure 6. Grid convergence study of the current model.

D. A Hall Thruster-Like Testcase

Before implementing this model into a Hall thruster plume simulation code, a Hall thruster-like testcase was constructed by Dragnea using a similar in 2-D axisymmetric hybrid model.[14] Figure 7 shows (a) magnetic field lines and (b) magnetic field strength throughout the computational domain. Fixed plasma potentials of 300 V and 0 V at the left (anode-like) and the right (cathode-like) boundaries, and zero-gradient conditions were applied at the top and the bottom boundaries (Figure 8a). Constant electron temperature (T_e = 25 eV) and electron number density (1e17 m^{-3}) were used. Since the current model is in 3-D, infinitely long boundaries were assumed in the *z*-direction. Figure 8 shows the plasma potential calculated using (a) 2-D axisymmetric model solution that serves as a true solution, and (b) 3-D finite volume model developed in this study.

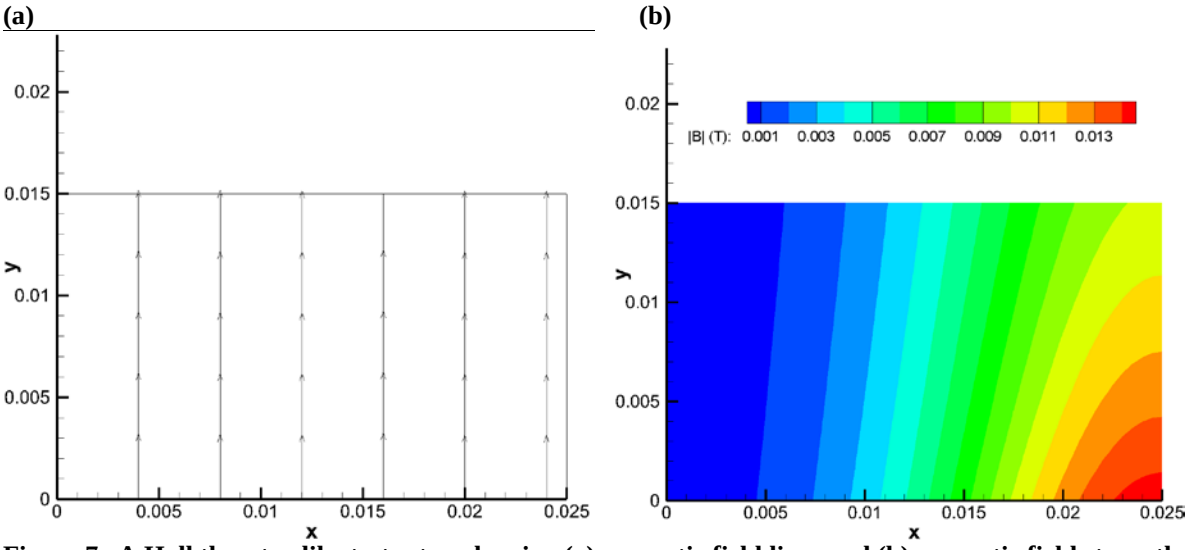

Figure 7. A Hall thruster-like test setup showing (a) magnetic field lines and (b) magnetic field strength

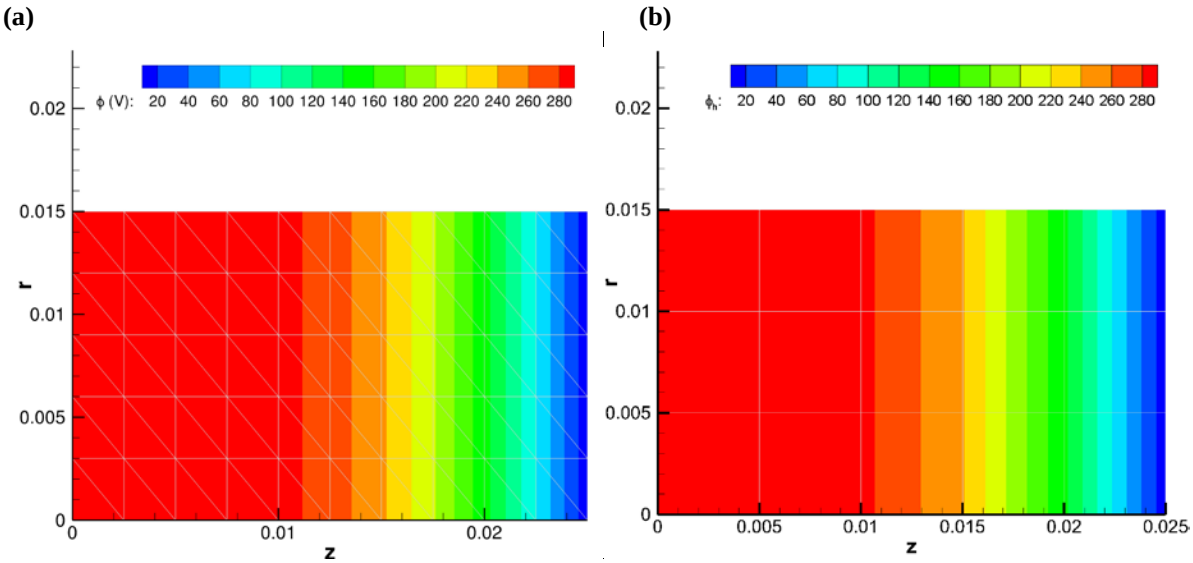

Figure 8. Plasma potential calculated using (a) 2-D axisymmetric finite element model from Ref. 12, and (b) the 3-D rectangular finite volume model in this study with constant values in z-direction.

V. Summary and Future Work

A 3-D electron fluid model has been developed as a stepping stone to ultimately better understand the electrical facility effects in a conducting vacuum chamber and to provide electron flux to solar arrays for spacecraft surface charging model. This unique formulation can include a representative magnetic field throughout an entire vacuum chamber domain for future Hall thruster plume simulations. This paper described the derivation and verification of the plasma potential solver. Current on-going work includes calculating electron current using various boundary conditions and conducting numerical experiments with various magnetic field strengths and topologies. In the near future, this model combined with a steady-state electron energy equation will be implemented in AFRL's plume code to study the electrical facility effects and spacecraft surface integration modeling. This model will be implemented in

a hybrid particle-fluid research framework developed by ARFL Edwards (TURF)[13] and used to simulate a Hall thruster plume in both a full vacuum chamber at NASA GRC and on-orbit with spacecraft geometry in the near future.

Acknowledgments

The authors would like to like to thank the Space Technology Mission Directorate through the Solar Electric Propulsion Technology Demonstration Mission Project for funding this project for the Advanced Electric Propulsion System.

References

[1]Walker, M.L.R., Hofer, R.R., and Gallimore, A.D., "The Effects of Nude Faraday Probe Design and Vacuum Facility Backpressure on the Measured Ion Current Density Profile of Hall Thruster Plumes," AIAA-2002-4253, 38th AIAA/ASME/SAE/ASEE *Joint Propulsion Conference*, Indianapolis, IN 7-10 July, 2002.

[2]Walker, M.L.R,Victor, A.L., Hofer, R.R., and Gallimore, A.D., "Effect of Backpressure on Ion Current Density Measurements in Hall Thruster Plumes," *Journal of Propulsion and Power*, Vol. 21, No. 3, 2005, pp. 408-415.

[3]Walker, M.L.R., "Effects of facility backpressure on the performance and plume of a Hall thruster," Ph.D. Dissertation, Aerospace Engineering Department, University of Michigan, Ann Arbor, MI, 2005.

[4]Reid, B.M., "The influence of neutral flow rate in the operation of Hall thrusters," Ph.D. Dissertation, Aerospace Engineering Department, University of Michigan, Ann Arbor, MI, 2009.

[5]Kamhawi, H., Huang, W., Haag, T., and Spektor, R., "Investigation of the effects of facility background pressure on the performance and voltage-current characteristics of the high voltage Hall accelerator," 50th AIAA/ASME/SAE/ASEE *Joint Propulsion Conference*, Cleveland, OH, 28-30 July 2014.

[6]Huang, W., Kamhawi, H., Lobbia, R.B., and Brown, D.L., "Effect of Background Pressure on the Plasma Oscillation Characteristics of the HiVHAc Hall Thruster," 50th AIAA/ASME/SAE/ASEE *Joint Propulsion Conference*, Cleveland, OH, 28-30 July 2014.

[7]Frieman, J.D., Walker, J.A., Walker, M.L., Khayms, V., and King, D.Q., "Electrical Facility Effects on Hall Thruster Cathode Coupling: Performance and Plume Properties," *Journal of Propulsion and Power*, Vol. 32, No. 1, 2015, pp. 251-264.

[8]Frieman, J.D., King, S.T., Walker, M.L., Khayms, V., and King, D., "Role of a Conducting Vacuum Chamber in the Hall Effect Thruster Electrical Circuit," *Journal of Propulsion and Power*, Vol. 30, No. 6, 2014, pp. 1471-1479.

[9]Boyd, I.D. and Yim, J.T., "Hall Thruster Plume Simulation Using a Detailed Hybrid Model," AIAA-2004–3952, 40th AIAA/ASME/SAE/ASEE Joint Propulsion Conference, 11-14 July, 2004, Fort Lauderdale, FL.

[10]Cai, C and Boyd, I.D., "3D Simulation of Plume Flows from a Cluster of Plasma Thrusters," AIAA-2005-4462, 36th AIAA Plasmadynamics and Lasers Conference, Toronto, Ontario, Canada, 6-9 June 2005.

[11]Brieda, L and VanGilder, D., "Multi-Domain Plasma Expansion Simulations Using a Particle-in-Cell Method," AIAA-2006-5023, 42nd AIAA/ASME/SAE/ASEE Joint Propulsion Conference, Sacramento, CA, 9-12 July, 2006.

[12]Choi, M., "Hybrid Simulation of Magnetic Field Effects in the Plume of a Hall Thruster," Space Propulsion, Rome, Italy, 2-6 May, 2016.

[13]Araki, S.J., and Barrie, A.C., "Electric Propulsion Plume Simulation Coupled with Spacecraft Charging," AIAA Propulsion and Energy Forum and Exposition, Cincinnati, OH, 9-11 July 2018.

[14]Dragnea, H.C. Hara, K., and Boyd, I.D., "A fully 2D Electron Fluid Model for Hall Thrusters," 8th Annual Gaseous Electronics Conference/9th International Conference on Reactive Plasmas/33rd Symposium on Plasma Processing, 2015.